Plasma Chemistry and Plasma Processing (2024) 44:1357–1368
https://doi.org/10.1007/s11090-023-10397-w

ORIGINAL PAPER

Plasma Catalytic Conversion of Nitrogen and Hydrogen to Ammonia Over Silico Alumino Phosphate (SAPO) Zeolites

Fnu Gorky[1] · Apolo Nambo[2] · Moises A. Carreon[3] · Maria L. Carreon[1]

Received: 18 June 2023 / Accepted: 9 September 2023 / Published online: 3 October 2023

Abstract

Herein, we demonstrate the catalytic activity of microporous Silico Alumino Phosphate (SAPOs) crystals for the assisted plasma synthesis of ammonia. SAPOs can aid as effective catalysts for the synthesis of ammonia via non-thermal plasma using an atmospheric dielectric barrier discharge (DBD) reactor. We studied three prototypical zeolites having crystallographic limiting pore apertures of 3.4 Å (SAPO-56), 3.8 Å (SAPO-34) and 3.9 Å (SAPO-11). We describe a fundamental insight on the effect of the Si/Al ratio and the pore size on ammonia synthesis rate for the different SAPOs. The resultant SAPO-11 displayed ammonia synthesis rates as high as 0.19 micromoles NH_3/ min m^2 at 20 watts, approximately 1.5 times better compared to other SAPOs. The results indicate that ammonia synthesis is promoted by a lower Si/Al ratio (< 0.25) of the SAPO. Moreover, we observed that SAPO-34 (3.8 Å) and SAPO-11 (3.9 Å) which allow diffusion of N_2 (3.6 Å) in to the pores lead to a higher ammonia yield. The lower intensity observed in optical emission spectroscopy (OES) for SAPO-34 suggests the diffusion of plasma activated species onto the surface and the pores. Proving the importance of porosity in plasma catalysis.

Graphical Abstract

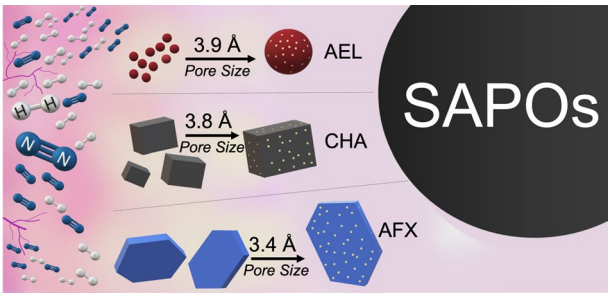

Keywords Non-thermal plasma · Plasma catalysis · Ammonia synthesis · SAPO crystals · Ammonia adsorption

Extended author information available on the last page of the article

Introduction

The production of ammonia is integral for food security due to its use in fertilizers. The typical industrial synthesis is currently done through the Haber–Bosch (HB) process typically at 500 ºC and 500 bar, which is the highest energy-consuming process in the chemical industry. Global ammonia production consumes 1–2% of the world's energy, 2–3% of the world's natural gas output, and emits 450 million metric tons of CO_2 annually [1, 2]. With such high energy and reaction condition requirements, the HB process is only economically viable at large-scale plants that demand enormous capital investments and access to continuous electric power to keep the process continuously running [3, 4]. Consequently, ammonia synthesis is currently centralized, hampering the access to farms in remote areas to affordable fertilizers. The inevitability of substituting fossil fuels and the climate change motivates to progress toward more sustainable methods for N_2 reduction based on clean energy. Electron-mediated technologies have currently gained attention for the sustainable production of ammonia. Thus, looking for an alternative is important to continue the production of sustainable ammonia to satiate the present demand.

In this respect, plasma catalysis offers a possible new alternative for small scale decentralized synthesis of ammonia. However, non-thermal plasma technology requires more knowledge of suitable materials that can take advantage of the rich gas chemistry offered. Currently, there is an increased interest in porous materials and the rational engineering of a catalyst for cold plasma environments is emerging as a highly promising strategy to lead to sustainable ammonia production [5–8]. Specifically, the presence of high energy electrons in plasmas can excite ground state gas molecules that then can react efficiently on the surface of selected materials at lower temperatures and pressures as compared to thermal catalysis [9]. In fact, it has been reported that the presence of a suitable active catalyst for plasma environments can enhance the ammonia production and selectivity [10–18].

With benefits such as low temperature and atmospheric pressure in plasma catalysis, there is the need to improve our current knowledge of optimum catalysts for such purpose.

Based on previous reports, MOFs with high surface areas exhibited high ammonia synthesis rates, however the catalyst stability degraded when subjected to multiple cycles in plasma environment showing amorphization [19]. The MOFs sensitivity arises due to presence of organic linkers in the backbone of the catalyst's structure [19, 20]. Hence, it is important to explore and tailor catalysts such as inorganic microporous catalysts with higher stability such as zeolites. The catalyst stability is an important feature to perform multiple cycles, making zeolites a potential candidate as catalyst for plasma catalytic ammonia synthesis.

Recently, the adsorption of ammonia over inorganic microporous materials have been explored, specifically the ammonia adsorption on the zeolite 4A during plasma catalytic ammonia synthesis which escalates the ammonia yield by reducing the ammonia decomposition in the plasma environment [6]. Furthermore, there is a need to have a better understanding on how different porous materials perform when exposed to plasma due to the occurrence of plasma awakened properties or interactions.

The use of crystalline microporous materials is highly appealing for plasma ammonia synthesis. Attributes that make them attractive for such application are (1) high thermal and chemical stability, (2) high surface area that increases the probability of active sites for reaction, (3) pore size within range for improved diffusion of guest molecules (reactants and products) during reaction, and (4) the possibility of geometrical electric field enhancement [21]. Recently, our group demonstrated the use of microporous crystalline materials,

including metal organic frameworks [20], and zeolites [20, 22, 23] as catalysts for the synthesis of ammonia via plasma. In these reports, we found that the surface area play an important role in the observed catalytic performance. In this contribution, we explore the plasma catalytic synergy between the pore size, and the Si/Al ratio influencing the synthesis of ammonia by employing three different pore apertures 3.4 Å (SAPO-56), 3.8 Å (SAPO-34) and 3.9 Å (SAPO-11) belonging to Silico Alumino Phosphate (SAPO) zeolite.

Experimental Methods

Synthesis of SAPOs

SAPO-56. The synthesis method for SAPO-56 was reported in our previous work [24]. It was crystallized via hydrothermal synthesis from a starting gel with the molar composition of SAPO-56 of 2TMHD : $0.6SiO_2$: $0.8Al_2O_3$: $1P_2O_5$: $40H_2O$. Briefly, a mixture of phosphoric acid, DI water, and aluminum hydroxide hydrate was stirred for 1 h at room temperature. Then, LUDOX AS-40 and TMHD were subsequently added to the solution and stirred for 24 h with a lid cover at room temperature. The resultant gel was transferred to a Teflon lined stainless steel autoclave and aged at 200 °C for 96 h. The autoclave was kept in the fume cupboard to cool down to room temperature. The solid gel was centrifugated and washed 3 × with DI water. The sample was dried at room temperature overnight before calcining at 400 °C for 20 h with a heating rate of 1 °C/min.

SAPO-34. We synthesized SAPO-34 crystals similarly to our previous report [25]. The starting gel ratio for SAPO-34 powder was $1Al_2O_3$: $1P_2O_5$: $0.3SiO_2$: 1TEAOH : 1.6DPA : $250H_2O$. Accordingly, the appropriate amount of aluminum isopropoxide was dissolved in DI water contained in a 100 mL beaker and allowed to become a homogenous solution by stirring for 1 h. Phosphoric acid was then added dropwise to the mixture and stirred for 2 h. Colloidal silica was also added to the solution and stirred for 3 h. Tetraethyl ammonium hydroxide (TEAOH) employed as a structure-directing agent (SDA) was added into the mixture. The solution was stirred for 30 min before adding dipropylamine, which was used as secondary structure directing agent. The beaker was then covered by a lid and kept at 50 °C on a hot plate for 3 days. The sample was aged at 220 °C for 6 h in a Teflon lined stainless steel autoclave. After cooling to room temperature, the resultant gel was centrifuged and washed 3 × with DI water before drying at ~ 100 °C in an oven overnight. The powder was calcined in an MDI tube furnace at 400 °C with a heating/cooling rate of 0.8 °C/min for 4 h in a continuous flowing air with a flowrate of 100 sccm.

SAPO-11. SAPO-11 was obtained from Chemie India Pvt. Ltd. Nandesari, Baroda, India.

Characterization Methods

The SAPO crystals were characterized by powder X-ray diffraction (XRD), with a Bruker Discovery D8 HR-XRD, with Cu Kα radiation (λ = 1.54 Å) ranging from 10 to 40° angles for confirming the XRD pattern on the employed catalyst. (See supplementary information Figure S1) JEOL JSM-7401F scanning electron microscope was used to study the morphology of the crystals. The Si/Al ratios were estimated with the XRF system (Bruker

Table 1 General properties of the SAPOs employed in this study

Catalyst		SAPO-34	SAPO-56	SAPO-11
Topology		CHA	AFX	AEL
Framework			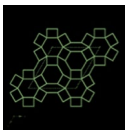	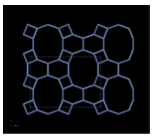
Crystal System		Trigonal	Hexagonal	Orthorhombic
Fresh Surface Area	(m^2/g)	425	598.3	178
Pore Size	Å	3.8	3.4	3.9
Pore Volume	(cm^3/g)	0.25	0.25	0.25
Avg. crystal size	(µm)	1–2	15–20	1.5
Si/Al	ratio	0.15	0.55	0.06

Topology: CHA = Chabazite; AFX = Silico-Aluminophosphate-fifty-six; AEL = Aluminophosphate-eleven

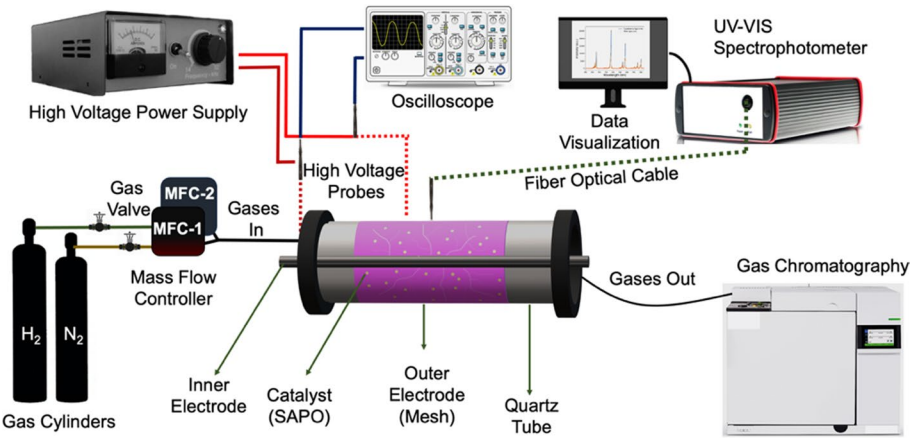

Fig. 1 Representation of the DBD reactor and equipment's employed in this study

AXS Tracer IV-SD). (See supplementary information Table S1.) The physico-chemical properties for employed catalysts are presented in Table 1.

Ammonia Synthesis Reaction Setup

The ammonia synthesis reaction on the studied SAPO crystals was performed in an *in-house* designed Dielectric Barrier Discharge (DBD) reactor [20, 26, 27]. This plasma reaction system can be divided into four major sections; (1) the catalyst packing zone, (2) the emission spectrum capture system (OES), (3) the oscilloscope and (4) the Gas Chromatograph (GC) for quantifying ammonia. The complete set up is shown in Fig. 1. To perform the tests, pure Nitrogen and Hydrogen cylinders were employed, they were connected to

the reactor through mass flow controllers. The exit of the reaction system was connected to a GC for online gas quantification. The quantification was performed using an Agilent 8860 A GC connected with a HP-PLOTU column (30 m × 0.32 mm × 10 µm) and hydrogen gas as carrier. The high voltage power supply was connected to the reactor using Litz wire and clips. The inner electrode made of tungsten rod (2.4 mm diameter) was placed at the center of the quartz tube with an I.D. of 4 mm and O.D. of 6.40 mm. The outer electrode made of tinned copper mesh acted as the ground electrode. The length of the plasma zone was ~ 6 cm. The gases flowed through the annular region and two quartz frits were placed carefully to avoid any material displacement and to do not cause any pressure increase. 100 mg of each SAPO were loaded as fine powder in the system. The SAPOs were packed in the overlap area between the inner and outer electrodes. The light emitted from the discharge was led through an optical system and the emission spectra of the glow region were measured at the center of the tube. The measurements were recorded using a dual channel UV–VIS-NIR spectrophotometer in scope mode (Avantes Inc., USB2000 Series). The spectral range was from 200 to 1100 nm, using a line grating of 600 lines/mm and resolution of 0.4 nm. A bifurcated fiber optic cable with 400 µm was employed. The experiments were carried out with a total flow rate of 25 sccm, the optimum flow rate for achieving the highest ammonia synthesis rate based on our previous investigations [22, 23] with different feed ratios including nitrogen rich 3:1 (N_2:H_2), equimolar 1:1(N_2:H_2), and hydrogen rich 1:3(N_2:H_2) content, at applied voltage of 12.1 ± 0.8 $kV_{pk\text{-}pk}$. The average bulk temperature during plasma catalytic operations was monitored using an Infrared thermometer (Fluke-62) at three different locations before averaging, also described in our previous report [27]. The reactor was connected to an oscilloscope to obtain the current and voltage waveforms. A Tektronix 2048 series oscilloscope was used along with a Tektronix P6015A high voltage probe having a 1000X voltage reducing rating. The current was measured by a 10X current reducing probe to get the waveforms. The energy delivered to the reactor was calculated based on these measurements.

Results and Discussion

The morphology of employed catalysts (SAPOs) was analyzed using Scanning Electron Microscopy (SEM). See Fig. 2. Figure 2a shows a SEM of SAPO-56 displaying large 15–20-micron hexagonal plate shapes, which is a major characteristic of SAPO-56 [28, 29]. Figure 2b shows a standard SEM of SAPO-34 crystals displaying small and uniform cubic shapes with sizes of 1–2 microns. Finally, Fig. 2c shows very small SAPO-11 crystals of less than 0.1 microns with spherical like morphologies forming aggregates of 1.5

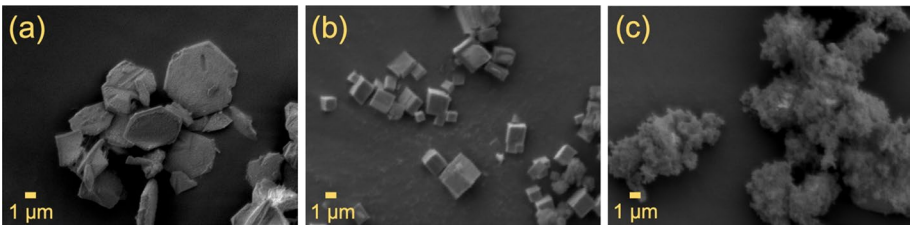

Fig. 2 SEM images for the fresh catalyst employed in this work, **a** SAPO-56, **b** SAPO-34, **c** SAPO-11

microns. Details on SEM for SAPOs after plasma exposure are provided in Figure S2 (Supplementary Information).

The XRD for the fresh samples is presented in Fig. 3. The XRD pattern displayed in Fig. 3 correspond to that of the literature and it can be observed that SAPO-11 present the lowest degree of crystallinity. Interestingly after plasma reaction the characteristic peaks for each zeolite showed a remarkable improvement in crystallinity by an increase in intensity. See supporting information Figure S1 for spent XRD data. The presented observation demonstrates the plasma-catalyst synergism experimentally, where the plasma active species collide with the zeolite surface and re-arrange the crystalline planes.

Plasma Catalytic Activity: Ammonia Synthesis

The plasma catalytic ammonia synthesis rates were conducted at different plasma powers ranging from 5–20 Watts to identify the best performing condition for the employed SAPOs. The reactions were repeated in triplicates and operated at 92 °C (Average bulk temperature) and atmospheric pressure. The best performance was observed at equimolar feed ratio (1:1) N_2:H_2. (All the feed ratios conducted are provided in Figure S3.) To understand the catalytic effect of the microporous materials and differentiate it from the only plasma effect, all the catalysts were tested at a total flow rate of 25 sccm as shown in Fig. 4. SAPO-11 (3.9 Å) displayed ammonia synthesis rates of 48.3 micromoles of NH_3/min gcat at high plasma power (20 Watts). While comparing the catalytic performance (at the same reaction conditions) for other catalysts reported by our group such as zeolite beta [23], zeolite 5A [23], alumina [23, 30], silica [23, 30] and ZIF-67 [20]. It is evident that SAPOs display higher ammonia synthesis rates at high plasma power and when data is normalized with surface area SAPO-11 shows a greater ammonia production per meter square than any other material here reported. When looking at the employed catalysts, it is observed that SAPO-34 (3.8 Å) and SAPO-11 (3.9 Å) displayed the highest performances at all the tested powers, both materials favoring the free path of Nitrogen (3.6 Å) through their pores. Another contributing factor to the higher performance of SAPO-11 could be its low crystallinity (higher entropy) providing more grain boundaries that could act as active sites for the plasma-activated species being generated in the gas bulk. Also reported in the literature and theoretically applied in sensors, grain boundary/defects facilitates effective

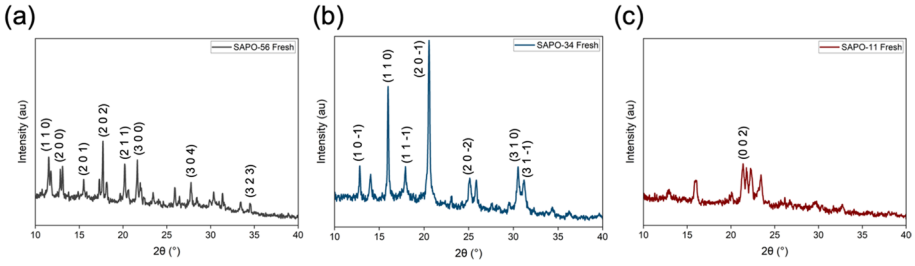

Fig. 3 X-ray diffraction pattern for the fresh catalysts employed in this work, **a** SAPO-56, **b** SAPO-34, **c** SAPO-11

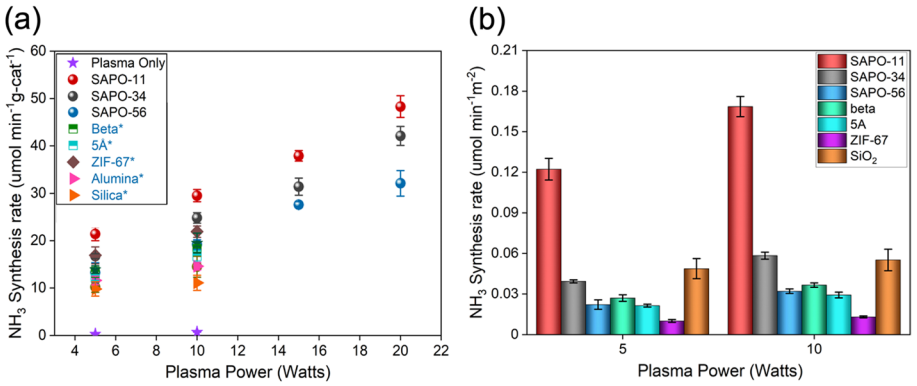

Fig. 4 **a** Ammonia synthesis rate performance normalized with amount of catalyst loaded for the studied SAPO crystals (this work) at 1:1 (N_2:H_2) feed ratio and plasma power (5–20 Watts), **b** Ammonia synthesis rate performance normalized with surface area for the studied SAPO crystals (this work) at 1:1 (N_2:H_2) feed ratio and plasma power (5–10 Watts)

electronic transport for catalytic reactions by generating large quantities of active sites for the absorption of ammonia molecules [11].

OES and Electrical Analysis

Optical emission spectra of the DBD N_2 and H_2 species were measured to get a better understanding of the role of the gas phase species in the plasma synthesis of ammonia. The collected emission spectra presented are for the equimolar feed ratio. We performed this analysis aiming to understand the behavior of plasma species with different SAPOs. Interestingly, Fig. 5a, b show the lowest intensity observed for Nitrogen and Vibrational Nitrogen species in the gas phase for SAPO-11 which delivered the highest ammonia synthesis rate. Further, Fig. 5c, d confirmed the presence of H_α Balmer and N_{atomic} species suggesting the dissociation of H_2 and N_2 by electron collision.

The low intensity observed for SAPO-11 could suggest that the excited species (NH and N_2, N_2^+, H_α, N_{atomic}) generated by the plasma excitation are diffusing through the pores and interact with the zeolite surface. The details for full OES spectrum and Lissajous curve can be found in Figure S4.

Plasma Catalytic Activity: Morphology and Acidity Effects

The pore size effect can be observed in Fig. 6 a, b. where the normalized ammonia synthesis rate is plotted against the pore size. It is denoted that above 3.6 Å the nitrogen can pass through the pores and the performance of the catalytic material is no longer limited by the pore size.

Once the pore size is not a limiting factor the ammonia synthesis seems to be directed by the nature of the material surface, for the case of the SAPO structure that can be denoted as the Si/Al ratio. When looking at the Si/Al ratio, we observed that the highest ammonia synthesis rate is observed in SAPO-11, with the lowest Si/Al ratio. It has been reported

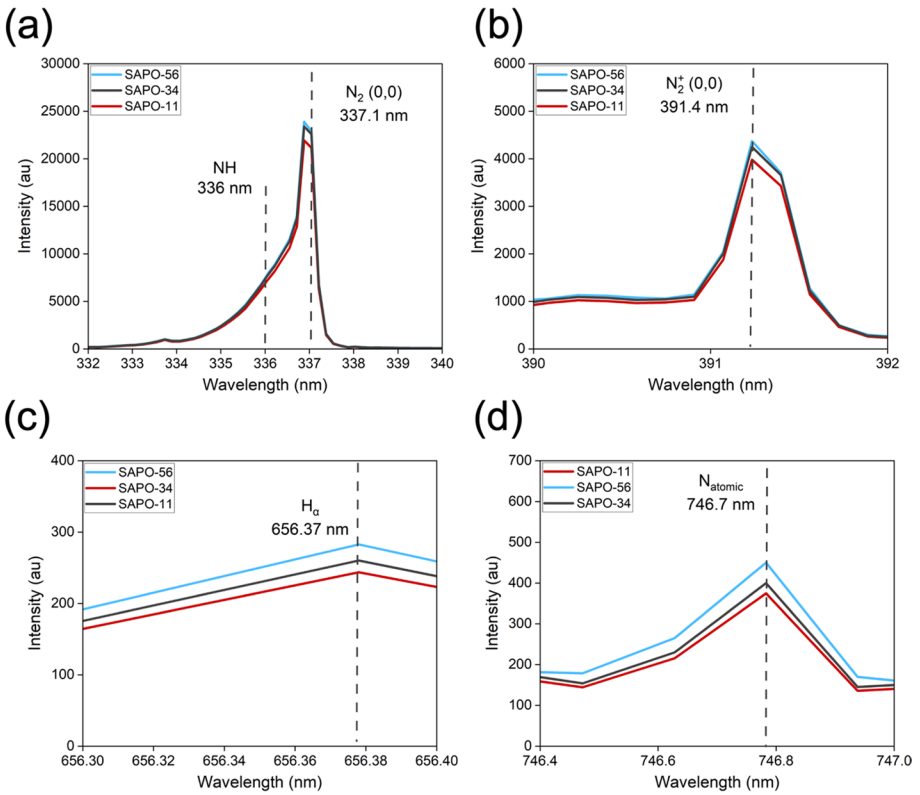

Fig. 5 Emission spectra collected during plasma catalytic ammonia synthesis at equimolar feed ratio N_2:H_2 ratio when employing **a** NH and N_2 band at 337.1 nm, **b** N_2^+ band at 391.4 nm, **c** H_α Balmer series 656.37 nm, **d** N_{atomic} (746.7 nm) for all employed catalysts in this work

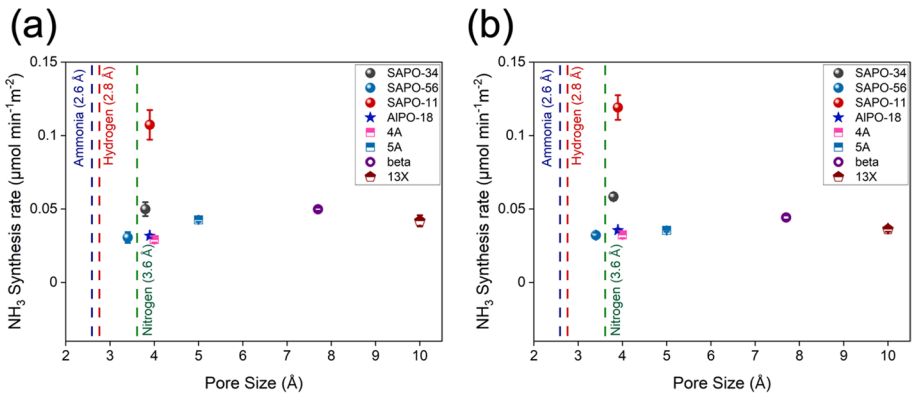

Fig. 6 Ammonia synthesis rate vs. Pore size (Å) evaluated at 1:1 (N_2:H_2) feed ratio at **a** 5 Watts vs. **b** 10 Watts plasma power and total flow rate of 25 sccm

that a lower value of the Si/Al ratio lead to greater acidity. Our measured Si/Al ratio for the studied zeolites can be found in the Supporting Information (see Table S1.) Acidity has been reported to improve the ammonia production in plasma catalysis [31]. During plasma-catalysis, it is well documented [18–21] that the formation of several important active species is done in the gas bulk. Thanks to the very nature of plasma the highly dependent material specific steps such as gas dissociation in a metal surface are not a critical step in plasma-catalysis. Hence materials such as zeolites with no metal active centers can be employed in plasma catalysis. In fact, the active sites in pristine SAPOs are dynamically distributed between Lewis Acid Sites (LAS) and Brønsted Acid Sites (BAS) driving the adsorption and recombination that governs the reaction kinetics in the plasma-catalysis systems. (see Table S2.). In the literature, it has been reported that the synergistic interaction between adsorbate and pristine zeolites such as SAPOs induces frustrated Lewis pair which further favors molecular adsorption of competitive polar adsorbates due to their ineffective orbital extension in their fixed framework [22].

Figure 7 displays the normalized ammonia synthesis rates using the measured surface areas (micromoles NH_3/ min m^2) vs Si/Al ratio. The highest synthesis rate for ammonia was observed over SAPO-11 at Si/Al of ~ 0.06, followed by SAPO-34 with a Si/Al of ~ 0.15.

The lowest ammonia synthesis rate for ammonia was observed over SAPO-56 having high Si/Al ratio (~ 0.45) with a small pore size that led to diffusion limitations that explain the lower performance observed. SAPOs exhibited remarkable performance compared to the materials employed in literature; see state-of-the-art table (Table S3.)

The Zeolite Lifetime

Plasma catalytic ammonia synthesis was carried out in three different cycles to compare the SAPOs stability at various plasma power (5–20 Watts). The ammonia synthesis performance was reduced at the 2nd and 3rd cycles among all SAPOs presented in Fig. 8. Interestingly, in the case of SAPO-11 that has the highest ammonia synthesis performance, the yield was reduced the most, dropping 21.63% in the 3rd cycle, followed by SAPO-56 with an average reduction of 19.05%. The catalytic performance was observed to be more stable in SAPO-34 among all zeolites, with an average reduction (%) of 13.95% at the 3rd

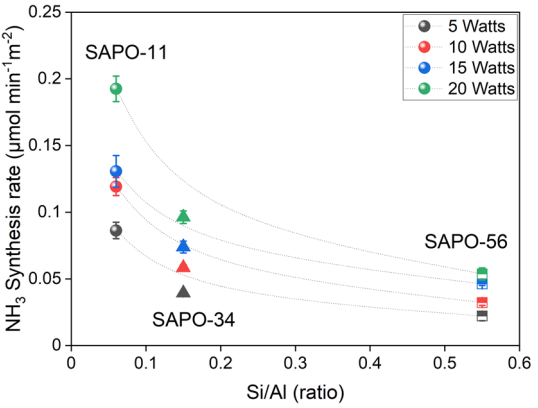

Fig. 7 Compares the ammonia synthesis rate vs measured Si/Al (ratio) for several catalysts evaluated at the same 1:1 (N_2:H_2) ratio when employing the same reaction system at 20 Watts plasma power

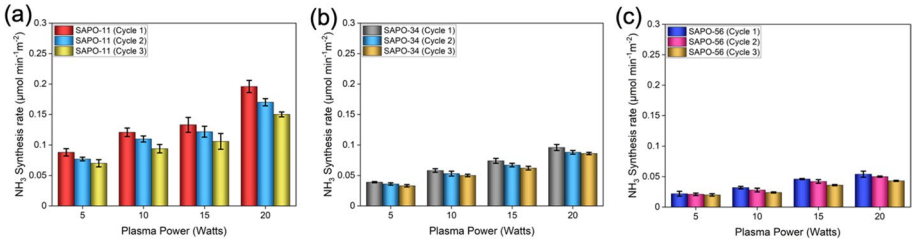

Fig. 8 Plasma catalytic ammonia synthesis performance with multiple cycles for employed catalyst **a** SAPO-11, **b** SAPO-34, **c** SAPO-56

cycle. The XRD patterns collected from spent catalyst (Figure S1) can be correlated with the catalytic stability, it can be observed that the more crystalline materials tend to be more stable resulting in a lower activity drop. The enhancement of crystallinity and surface rearrangement could increase the stability of the catalytic performance and it is more evident in SAPO-56. In the literature, it has been reported that after plasma exposure, the number of weak acid sites in zeolites decreases [32]. Specifically, for the case of long plasma exposure (100 h) a reduction in the number of Brønsted acid sites and an increase in the number of Lewis acid sites in zeolites (ZSM-5) is reported [33], resulting in an evident lower performance in ammonia synthesis rate after multiple cycles, as presented in this work.

Conclusions

Herein, we demonstrate the plasma catalytic synergism between SAPOs with different textural properties and their influence on ammonia synthesis rate under atmospheric DBD plasma discharge. The highest normalized ammonia synthesis rate was observed for SAPO-11 (3.9 Å) followed by SAPO-34 (3.8 Å), both materials with pore sizes above the kinetic diameter of nitrogen (3.6 Å). From OES we observed a low intensity for N_2, H_α and N_{atomic} lines suggesting the diffusion of plasma activated species inside the pores and accessing the surface area resulting in greater ammonia production. Both surface area and Si/Al ratio played an important role towards ammonia formation. With competitive pore sizes, 3.8 Å (SAPO-34) vs 3.9 Å (SAPO-11), the Si/Al played a major role in the superior performance of SAPO-11. The presented work provides experimental analysis on prototypical SAPOs which will aid in further tailoring catalysts for designing an optimum complex material such as membranes for plasma catalytic ammonia synthesis.

Supplementary Information The online version contains supplementary material available at https://doi.org/10.1007/s11090-023-10397-w.

Acknowledgements Maria L. Carreon acknowledges the Department of Energy Office of Science DE-SC0023261, NSF-CBET award No.1947303, and NSF-CAREER award No. 2235247. The authors want to express their gratitude to the late Dr. Moises A. Carreon, an expert on zeolites, without whom this project would never have been possible.

Author Contributions FG: Performed ammonia synthesis experiments; Formal Analysis, Methodology, Reviewing and Editing; AN: XRD characterization of zeolites; results analysis, writing and editing; MAC: synthesis and characterization of zeolites; MLC: Project conceptualization, supervision, funding acquisition, project administration, reviewing and editing.

Funding Department of Energy Office of Science DE-SC0023261, NSF-CBET award No. 2203166, and NSF-CAREER award No. 2235247.

Data Availability A reasonable request to the corresponding authors may permit the data used to support the results of this study.

Declarations

Conflict of interest The authors declare no competing interests.

Ethical Approval All experiments in this study were carried out in adherence to ethical standards, and no ethical concerns were encountered during the course of the experiments or preparation of this manuscript.

References

1. Tanabe Y, Nishibayashi Y (2013) Developing more sustainable processes for ammonia synthesis. Coord Chem Rev 257:2551–2564
2. http://ictpost.com/global-ammonia-capacity-to-reach-250-million-tons-per-year-by-2018/, Global Ammonia Capacity to reach 250 million tons per year by 2018, in, 2015
3. Erisman JW, Sutton MA, Galloway J, Klimont Z, Winiwarter W (2008) How a century of ammonia synthesis changed the world. Nat Geosci 1:636
4. R. Schlogl, Ammonia Synthesis in: "Handbook of Heterogeneous Catalysis", Department of Inorganic Chemistry, Fritz-Haber-Institute of the MPG, Germany (1991)
5. Carreon ML (2019) Plasma catalytic ammonia synthesis: state of the art and future directions. J Phys D 52:483001
6. Rouwenhorst KHR, Mani S, Lefferts L (2022) Improving the energy yield of plasma-based ammonia synthesis with in situ adsorption. ACS Sustain Chem Eng 10:1994–2000
7. Wang Y, Yang W, Xu S, Zhao S, Chen G, Weidenkaff A, Hardacre C, Fan X, Huang J, Tu X (2022) Shielding protection by mesoporous catalysts for improving plasma-catalytic ambient ammonia synthesis. J Am Chem Soc 144:12020–12031
8. Chen Z, Jaiswal S, Diallo A, Sundaresan S, Koel BE (2022) Effect of porous catalyst support on plasma-assisted catalysis for ammonia synthesis. J Phys Chem A 126:8741–8752
9. Neyts EC, Ostrikov K, Sunkara MK, Bogaerts A (2015) Plasma catalysis: synergistic effects at the nanoscale. Chem Rev 115:13408–13446
10. Mehta P, Barboun P, Herrera FA, Kim J, Rumbach P, Go DB, Hicks JC, Schneider WF (2018) Overcoming ammonia synthesis scaling relations with plasma-enabled catalysis. Nat Catal 1:269–275
11. Barboun P, Mehta P, Herrera FA, Go DB, Schneider WF, Hicks JC (2019) Distinguishing plasma contributions to catalyst performance in plasma-assisted ammonia synthesis. ACS Sustain Chem Eng 7:8621–8630
12. Van't Veer K, Reniers F, Bogaerts (2020) Zero-dimensional modeling of unpacked and packed bed dielectric barrier discharges: the role of vibrational kinetics in ammonia synthesis. Plasma Sources Sci Technol 29:045020
13. Herrera FA, Brown GH, Barboun P, Turan N, Mehta P, Schneider WF, Hicks JC, Go DB (2019) The impact of transition metal catalysts on macroscopic dielectric barrier discharge (DBD) characteristics in an ammonia synthesis plasma catalysis reactor. J Phys D 52:224002
14. Hong J, Steven P, Anthony B, Murphy (2018) Plasma catalysis as an alternative route for ammonia production: status, mechanisms, and prospects for progress. ACS Sustain Chem Eng 6:15–31
15. Hong J, Prawer S, Murphy AB (2014) Production of ammonia by heterogeneous catalysis in a packed-bed dielectric-barrier discharge: influence of argon addition and voltage. IEEE Plasma Sci 42:2338–2339
16. Patil BS, Van Kaathoven ASR, Peeters FJJ, Cherkasov N, Lang J, Wang Q, Hessel V (2020) Deciphering the synergy between plasma and catalyst support for ammonia synthesis in a packed dielectric barrier discharge reactor. J Phys D 53:144003
17. Peng P, Li Y, Cheng Y, Deng S, Chen P, Ruan R (2016) Atmospheric pressure ammonia synthesis using non-thermal plasma assisted catalysis. Plasma Chem Plasma Process 36:1201–1210
18. Akay G, Zhang K (2017) Process intensification in ammonia synthesis using novel coassembled supported microporous catalysts promoted by nonthermal plasma. Ind Eng Chem Res 56:457–468
19. Shah J, Wu T, Lucero J, Carreon MA, Carreon ML (2018) Nonthermal plasma synthesis of ammonia over Ni-MOF-74. ACS Sustain Chem Eng 7:377–383

20. Gorky F, Lucero JM, Crawford JM, Blake B, Carreon MA, Carreon ML (2021) Plasma-induced catalytic conversion of nitrogen and hydrogen to ammonia over zeolitic imidazolate frameworks ZIF-8 and ZIF-67. ACS Appl Mater Interfaces 13:21338–21348
21. Kruszelnicki J, Engeling KW, Foster JE, Kushner MJ (2020) Interactions between atmospheric pressure plasmas and metallic catalyst particles in packed bed reactors. J Phys D Appl Phys 54:104001
22. Shah JR, Gorky F, Lucero J, Carreon MA, Carreon ML (2020) Ammonia synthesis via atmospheric plasma catalysis: zeolite 5A, a case of study. Ind Eng Chem Res 59:5167–5176
23. Gorky F, Carreon MA, Carreon ML (2020) Experimental strategies to increase ammonia yield in plasma catalysis over LTA and BEA zeolites. IOP SciNotes 1:024801
24. Xie Z, Zhu M, Nambo A, Jasinski JB, Carreon MA (2013) Microwave-assisted synthesized SAPO-56 as a catalyst in the conversion of CO_2 to cyclic carbonates. Dalton Trans 42:6732–6735
25. J.L. Falconer, M.A. Carreon, S. Li, R.D. Noble, Synthesis of zeolites and zeolite membranes using multiple structure directing agents, in, U.S. Patents, US 8,302,782 B2, 2012.
26. Gorky F, Nambo A, Carreon ML (2021) Cold plasma-metal organic framework MOF-177 breathable system for atmospheric remediation. J CO2 Utilization 51:101642
27. Gorky F, Nguyen HM, Krishnan K, Lucero JM, Carreon ML, Carreon MA (2023) Plasma-induced desorption of methane and carbon dioxide over silico alumino phosphate zeolites. ACS Appl Energy Mater 6:4380–4389
28. Wilson ST, Broach RW, Blackwell CS, Bateman CA, McGuire NK, Kirchner RM (1999) Synthesis, characterization and structure of SAPO-56, a member of the ABC double-six-ring family of materials with stacking sequence AABBCCBB. Microporous Mesoporous Mater 28:125–137
29. Wu T, Feng X, Carreon ML, Carreon MA (2017) Synthesis of SAPO-56 with controlled crystal size. J Nanopart Res 19:1–8
30. Gorky F, Best A, Jasinski J, Allen BJ, Alba-Rubio AC, Carreon ML (2020) Plasma catalytic ammonia synthesis on Ni nanoparticles: the size effect. J Catal 393:369–380
31. Wang Y, Craven M, Yu X, Ding J, Bryant P, Huang J, Tu X (2019) Plasma-enhanced catalytic synthesis of ammonia over a Ni/Al2O3 catalyst at near-room temperature: insights into the importance of the catalyst surface on the reaction mechanism. ACS Catal 9:10780–10793
32. Li G, Foo C, Yi X, Chen W, Zhao P, Gao P, Yoskamtorn T, Xiao Y, Day S, Tang CC (2021) Induced active sites by adsorbate in zeotype materials. J Am Chem Soc 143:8761–8771
33. Li Y, Su X, Maximov AL, Bai X, Wang Y, Wang W, Kolesnichenko NV, Bukina ZM, Wu W (2020) Highly selective MTO reaction over a nanosized ZSM-5 zeolite modified by Fe via the low-temperature dielectric barrier discharge plasma method. Russ J Appl Chem 93:137–148

Authors and Affiliations

Fnu Gorky[1] · Apolo Nambo[2] · Moises A. Carreon[3] · Maria L. Carreon[1]

✉ Maria L. Carreon
maria_carreon@uml.edu

[1] Mechanical Engineering Department, University of Massachusetts Lowell, 1 University Avenue, Lowell, MA 01854, USA

[2] Bert Thin Films, LLC, 625 Myrtle St, Louisville, KY 40298, USA

[3] Chemical and Biological Engineering Department, Colorado School of Mines, 1613 Illinois Street, Golden, CO 8040, USA